




# Flow-enhanced vascularization and maturation of kidney organoids in vitro

Kimberly A. Homan<sup>1,5</sup>, Navin Gupta<sup>2,3,4,5</sup>, Katharina T. Kroll<sup>1</sup> , David B. Kolesky<sup>1</sup>, Mark Skylar-Scott<sup>1</sup>, Tomoya Miyoshi<sup>2</sup>, Donald Mau<sup>1</sup>, M. Todd Valerius<sup>2,3,4</sup>, Thomas Ferrante<sup>1</sup>, Joseph V. Bonventre<sup>2,3,4</sup>, Jennifer A. Lewis<sup>1,3,6\*</sup>  and Ryuji Morizane<sup>1,2,3,4,6\*</sup> 

**Kidney organoids derived from human pluripotent stem cells have glomerular- and tubular-like compartments that are largely avascular and immature in static culture. Here we report an in vitro method for culturing kidney organoids under flow on millifluidic chips, which expands their endogenous pool of endothelial progenitor cells and generates vascular networks with perfusable lumens surrounded by mural cells. We found that vascularized kidney organoids cultured under flow had more mature podocyte and tubular compartments with enhanced cellular polarity and adult gene expression compared with that in static controls. Glomerular vascular development progressed through intermediate stages akin to those involved in the embryonic mammalian kidney's formation of capillary loops abutting foot processes. The association of vessels with these compartments was reduced after disruption of the endogenous VEGF gradient. The ability to induce substantial vascularization and morphological maturation of kidney organoids in vitro under flow opens new avenues for studies of kidney development, disease, and regeneration.**

The kidney continuously filters blood and maintains fluid homeostasis. These functions rely on specialized glomerular and tubular tissue compartments integrated with a complex vascular network. Although kidney organoids have such compartments<sup>1–8</sup>, their vasculature development—for example, the formation of PECAM1<sup>+</sup> vascular networks with luminal architecture—is limited in static culture<sup>3,9,10</sup>. Further, gene expression in podocytes and tubular epithelial cells in static organoids is reflective of less mature renal tissue compared with that of human adult kidneys described in published work<sup>3,9</sup>. To date, researchers have depended on animal transplantation to produce kidney organoids with a perfusable vasculature that facilitates nephron epithelial maturation<sup>10–12</sup>. However, the reliance on an animal host limits both the scalability and the translation of organoid-based approaches, particularly for in vitro applications.

Given that multilineage communication with vasculature is implicated in epithelial maturation in vivo<sup>13</sup>, we posit that enhanced vascularization and maturation may be promoted in human pluripotent stem cell (hPSC)-derived human kidney tissue in vitro when it is subjected to environmental cues. To test our hypothesis, we developed a millifluidic culture system to probe the effects of extracellular matrix (ECM), media composition, fluidic shear stress (FSS), and coculture with human endothelial cells on the in vitro development of kidney organoids.

## Results

**Developing kidney organoids exhibit enhanced vascularization under flow.** In our 3D-printed millifluidic chips, we subjected organoids to superfusion (flow over their top surface) with a controlled wall shear (i.e., FSS; Fig. 1a (top), Supplementary Fig. 1). The developing kidney organoids adhered to and became partially

embedded in an ~1-mm-thick layer of gelatin–fibrin (gelbrin) ECM coating the bottom of the printed chip<sup>14,15</sup>, which allowed fluid to freely flow through the gap (2.6 mm in height) between the ECM surface and the upper chip housing (Supplementary Fig. 1). The adherent gelbrin matrix led to enhanced peripheral expression of the vascular marker PECAM1 and its precursor, MCAM<sup>16</sup>, within 1 week in static conditions, compared with expression in nonadherent matrices (e.g., glass, plastic, fibrin with or without collagen type 1) (Fig. 1b, Supplementary Fig. 2a–f). We tested several media compositions, as well as coculture with primary human endothelia with or without fibroblasts, and found that most conditions inhibited nephron formation or did not enhance vascularization under fluid flow (Supplementary Figs. 2g–i and 3). A low FBS concentration of 1.5%, typically used in endothelial culture media, permitted nephrogenesis and enhanced vascular network formation in developing kidney organoids under static conditions (Supplementary Fig. 2h, i).

To determine the effects of fluid flow, we placed developing kidney organoids on the adherent gelbrin layer and superfused them overnight with basal organoid media supplemented with 1.5% FBS in a closed-loop system over a range of flow rates from 0.04 ml/min (low FSS; ~0.0001 dyn/cm<sup>2</sup>) to 1–4.27 ml/min (high FSS; 0.008–0.035 dyn/cm<sup>2</sup>) while continuing the published differentiation protocol<sup>1,2</sup> (Fig. 1a, bottom). We observed enhanced formation of MCAM<sup>+</sup> and PECAM1<sup>+</sup> vascular networks in organoids cultured in vitro under high FSS after 10 d of perfusion (differentiation day 21), with nephrons forming over time (Fig. 1c–l, Supplementary Video 1). To quantify their vascularization, we evaluated confocal images of whole organoids using the AngioTool plugin in ImageJ<sup>17</sup>. We found that the PECAM1<sup>+</sup> vasculature of organoids cultured under high FSS showed a fivefold increase in vessel percent area compared with that of organoids cultured under low FSS (Fig. 1m,

<sup>1</sup>Wyss Institute for Biologically Inspired Engineering, Harvard University, Cambridge, MA, USA. <sup>2</sup>Renal Division, Brigham and Women's Hospital, Boston, MA, USA. <sup>3</sup>Harvard Stem Cell Institute, Cambridge, MA, USA. <sup>4</sup>Department of Medicine, Harvard Medical School, Boston, MA, USA.

<sup>5</sup>These authors contributed equally: Kimberly A. Homan, Navin Gupta. <sup>6</sup>These authors jointly supervised this work: Jennifer A. Lewis, Ryuji Morizane.

\*e-mail: [jalewis@seas.harvard.edu](mailto:jalewis@seas.harvard.edu); [morizane@da2.so-net.ne.jp](mailto:morizane@da2.so-net.ne.jp)

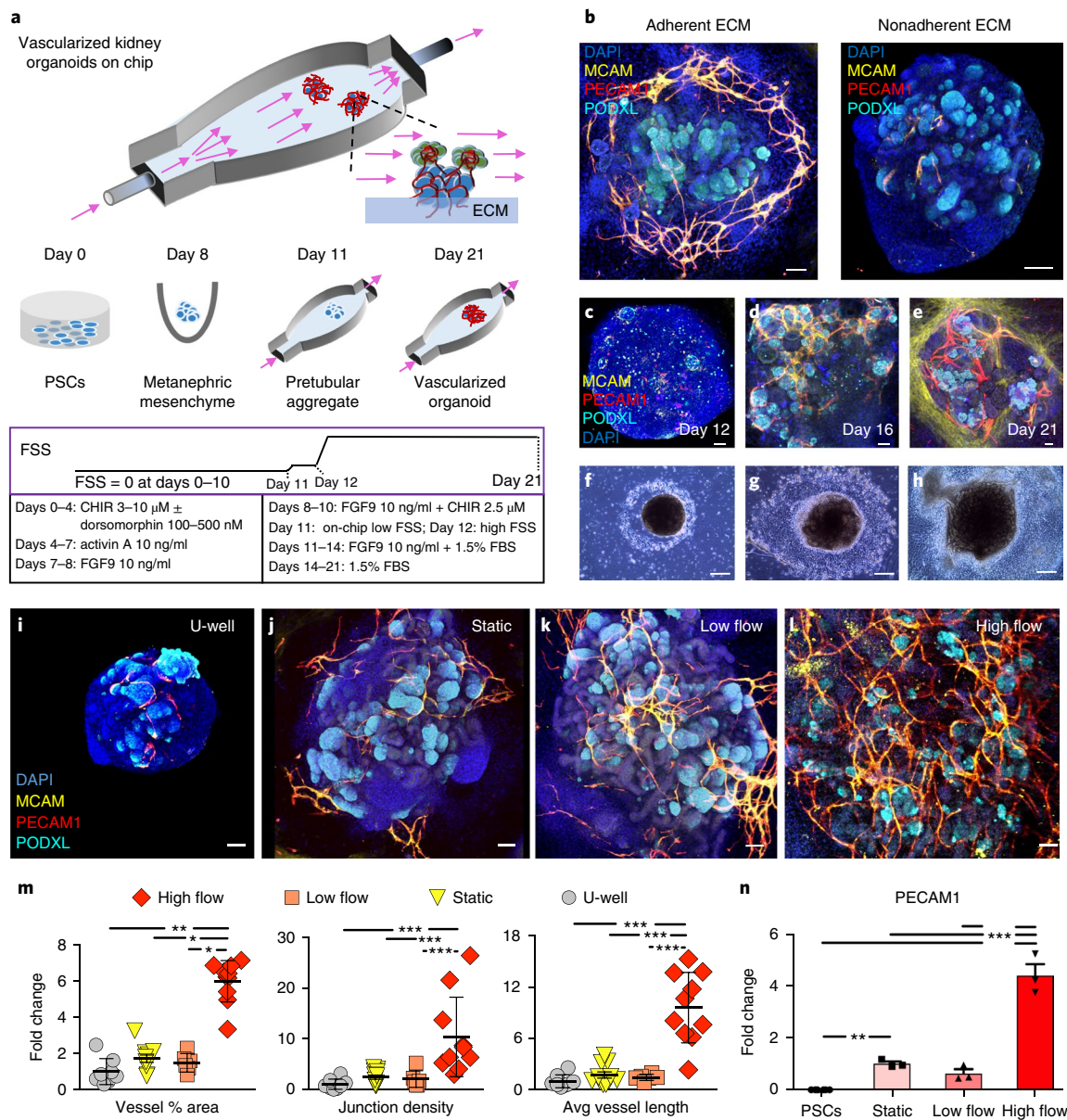


**Fig. 1 | Developing kidney organoids cultured in vitro under high fluid flow exhibit enhanced vascularization during nephrogenesis.** **a**, Developing renal organoids are placed on an engineered ECM, housed within a perfusable millifluidic chip, and subjected to controlled FSS. Differentiation days and culture conditions are indicated in the middle and bottom parts of the panel. Organoids not drawn to scale. **b**, Organoids grown on adherent or nonadherent ECM and stained for DNA, MCAM, PECAM1, and PODXL. Scale bars, 100  $\mu\text{m}$ . **c–h**, Immunostaining of whole-mount organoids (**c–e**) and representative phase contrast images of entire organoids (**f–h**) cultured under high FSS (days 12–21). Scale bars, 50  $\mu\text{m}$  (**c–e**) or 300  $\mu\text{m}$  (**f–h**). Perfusion direction is left to right. **i–l**, Confocal 3D renderings for vascular markers in whole-mount organoids cultured under static U-well, static engineered ECM, low-FSS, and high-FSS conditions. Scale bars, 100  $\mu\text{m}$ . **m**, AngioTool outputs of the abundance and character of vasculature, reported as a fold change relative to the U-well condition. We used biological replicates of 8, 11, 6, and 10 per condition (U-well, static, low flow, and high flow, respectively) in experiments with organoids derived from both induced pluripotent stem cells and human embryonic stem cells; each entire organoid represents one replicate (individual symbols), and data are plotted as mean  $\pm$  s.d. **n**, qPCR measurements of PECAM1 expression under various growth conditions. Data are plotted as mean  $\pm$  s.d. Each individual symbol represents three technical replicates on RNA pooled from 6 organoids (biological replicates) per condition. DAPI, 4',6-diamidino-2-phenylindole; PECAM1, CD31; MCAM, CD146; KDR, FLK1; PODXL, podocalyxin; CDH1, E-cadherin; CHIR, CHIR99021; FGF9, fibroblast growth factor 9. Statistical significance was attributed to values of  $P < 0.05$  as determined by one-way (**m**) or two-way (**n**) ANOVA with Tukey's multiple-comparisons test. \* $P < 0.05$ , \*\* $P < 0.01$ , \*\*\* $P < 0.001$ .

Supplementary Fig. 4). Similarly, we found that the PECAM1<sup>+</sup> vasculature showed a tenfold increase in junctional density (i.e., branch points per unit area) and average vessel length (i.e., interjunctional distance) under high FSS compared with that of organoids cultured in static or low-FSS conditions (Fig. 1m). Concomitantly, PECAM1

transcripts were fivefold upregulated under high FSS relative to expression in controls (Fig. 1n). Note that such differences cannot be attributed solely to variations in media volume, as organoids cultured under high FSS with either 0.2 ml or 1 ml of media per organoid in our closed-loop system did not show statistically



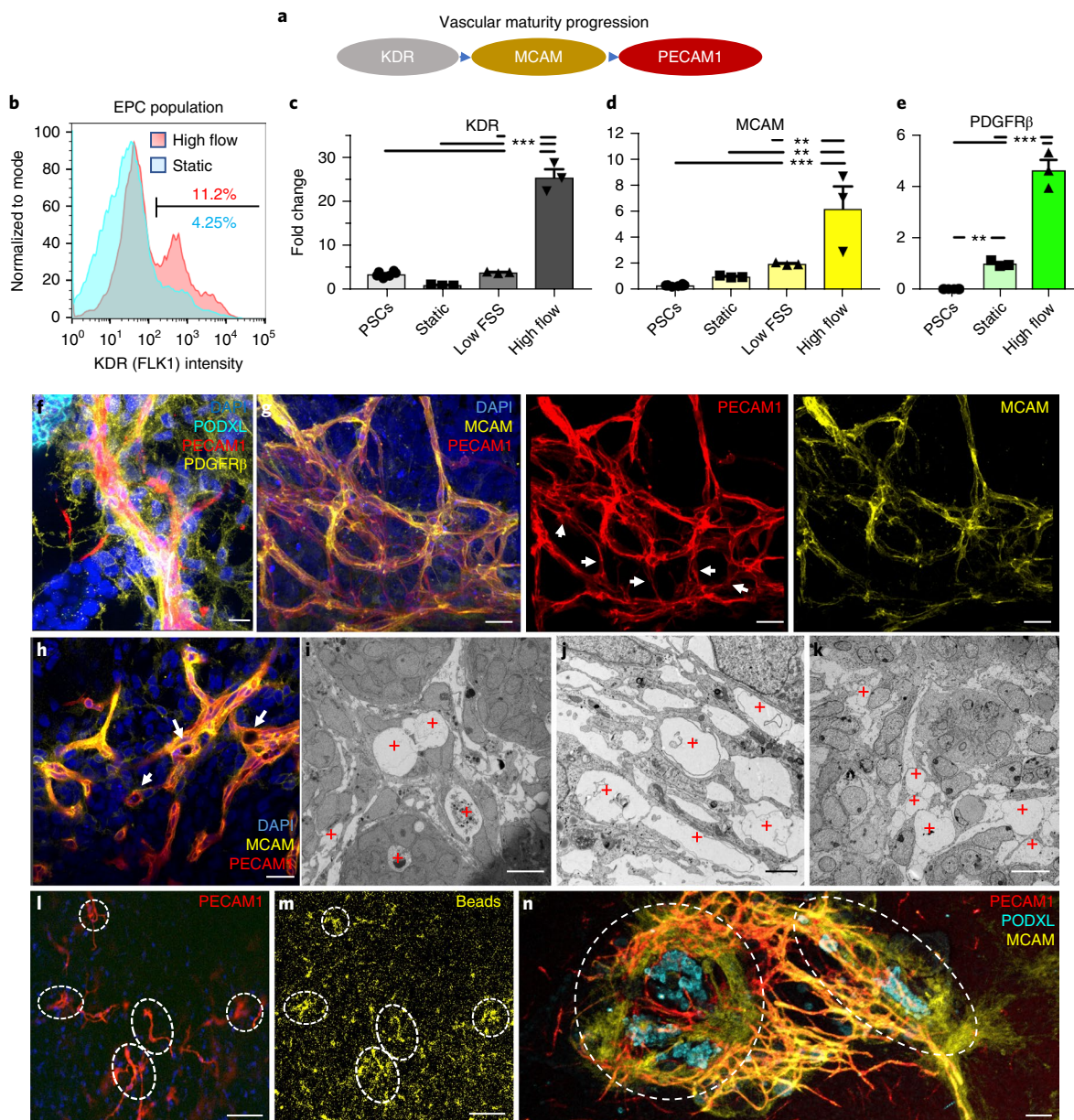


**Fig. 2 | Intra- and interorganoid vascular networks with perfusable lumens supported by mural cells are observed for kidney organoids cultured under high flow in vitro.** **a**, Diagram of endothelial maturation in developing kidneys in vivo, from progenitor cells to sustained terminal marker expression. **b**, Flow cytometry of dissociated whole organoids on day 21. EPCs were FLK1<sup>+</sup>. **c,d**, qPCR of endothelial cell markers in developing organoids at day 21. **e**, qPCR of PDGFRβ in developing organoids at day 21. Individual symbols in **c–e** represent three technical replicates on RNA pooled from 6 organoids (biological replicates) per condition. All data are plotted as mean ± s.d. **f**, Immunostaining for PODXL, PECAM1, and PDGFRβ in organoids under high FSS. Scale bar, 15 μm. **g**, Confocal 3D renderings of vascular markers within whole-mount organoids. Scale bars, 30 μm. White arrows highlight areas that are PECAM1<sup>+</sup>MCAM<sup>+</sup>. **h**, A single z-slice from **g** in which white arrows highlight open lumens. Scale bar, 30 μm. **i–k**, Transmission electron microscopy images showing circular openings encompassed by a thin membrane that reflect vascular lumens for kidney organoids subjected to high FSS (**i,j**) and E14.5 mouse embryonic kidney in vivo (**k**). Red plus signs indicate vascular lumens. Scale bars, 10 μm (**i,k**) or 2 μm (**j**). **l,m**, Z-slice at the base of a kidney organoid cultured under high FSS, showing the vascular network (**l**) and the accumulation of fluorescent beads within the vascular network (**m**). Scale bars, 100 μm. **n**, Confocal 3D rendering of bridging between two adjacent whole organoids (outlined by dashed white lines). Scale bar, 100 μm. DAPI, 4',6-diamidino-2-phenylindole; PECAM1, CD31; MCAM, CD146; KDR, FLK1; PODXL, podocalyxin; PDGFRβ, platelet-derived growth factor receptor-β. Statistical significance (**c–e**) was attributed to values of  $P < 0.05$  as determined by one-way ANOVA with Tukey's multiple-comparisons test. \*\* $P < 0.01$ , \*\*\* $P < 0.001$ .

significant differences in their vasculature ( $P > 0.05$ , two-way analysis of variance (ANOVA) with Tukey's multiple-comparisons test; Supplementary Fig. 5). Together, these observations suggest that FSS is a critical environmental cue that facilitates the vascularization of kidney organoids in vitro.

**Perfusable vessels form in developing kidney organoids under flow.** During kidney development, vascular formation is believed to arise via a combination of vasculogenesis (i.e., de novo formation of blood vessels through the differentiation and coalescence of endothelial progenitor cells (EPCs)) and angiogenesis (i.e., the formation

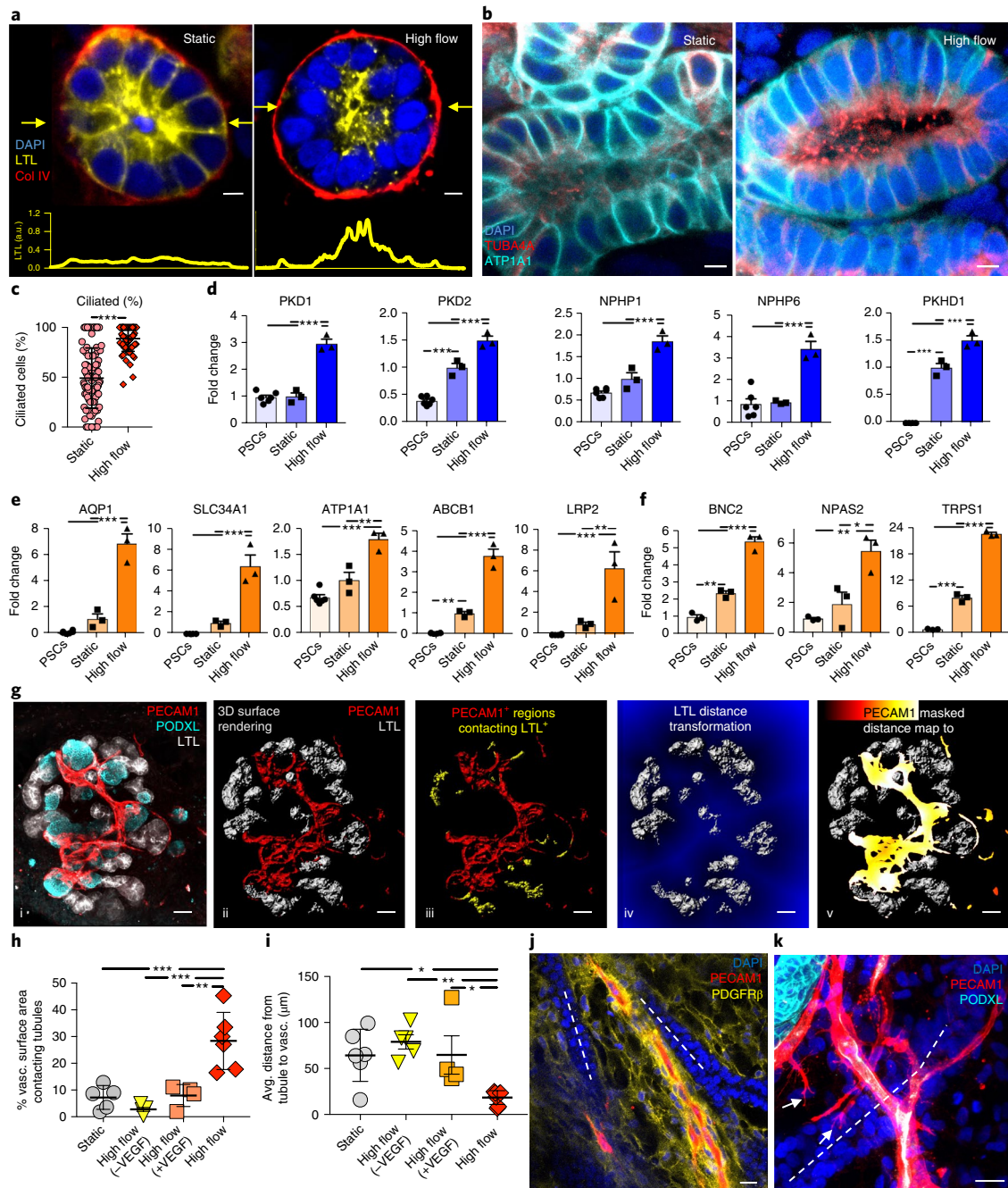


**Fig. 3 | Tubular epithelia mature and undergo morphogenesis to become a polarized, ciliated compartment in contact with vasculature in response to high-flow conditions on chip.** **a**, Expression of collagen IV and LTL in tubule cross-sections under static and high-flow conditions at day 21. Scale bars, 5 μm. The plots in yellow at the bottom show the intensity of LTL across a line scan denoted by yellow arrows in the images above. **b**, Tubule cross-sections showing the ciliary marker TUBA4A and expression of ATP1A1 (Na/K ATPase subunit-α1) under static versus high-flow conditions on chip on day 21. Scale bars, 5 μm. **c**, The percentage of ciliated cells under static ( $n=101$  cells) and high-flow ( $n=64$  cells) conditions. Samples were determined as a field of view in an LTL<sup>+</sup> tubule where at least 8 cells could be viewed in cross-section. **d–f**, qPCR of ciliary markers, solute transporters, drug transporters, and adult transcription factors on day 21 under the indicated growth conditions. **g**, Whole-organoid 3D confocal imaging stacks (i) of a representative high-flow sample are used to demonstrate the analysis method for the association of tubules with vasculature in Imaris 3D surface rendering (ii and iii) and distance transformation software (iv and v). Scale bars, 50 μm. **h**, The percentage of vasculature (vasc.) surface area overlapping with LTL<sup>+</sup> tubules within 1 voxel under the indicated growth conditions. **i**, The average distance in 3D between the vasculature and the tubules. Data in **h,i** represent biological replicates, or whole organoids, of 6, 5, 4, and 6 per condition (static, high flow (-VEGF), high flow (+VEGF), and high flow, respectively). **j,k**, Immunostaining for the indicated markers in transverse (**j**) and longitudinal (**k**) planes in high flow at day 21. Scale bars, 20 μm. DAPI, 4',6-diamidino-2-phenylindole; LTL, *Lotus tetragonolobus* lectin; PECAM1, CD31; PODXL, podocalyxin; TUBA4A, tubulin-α4a; AQP1, aquaporin 1; SLC34A1, Na/P cotransporter; ATP1A1, Na/K ATPase; ABCB1, MDR1; LRP2, megalin; BNC2, basonucin 2; NPAS2, neuronal PAS domain protein 2; TRPS1, transcription repressor GATA binding 1; PKD1, polycystin 1; PKD2, polycystin 2; NPHP1, nephrocystin 1; NPHP6, nephrocystin 6; PKHD1, fibrocystin. All data are plotted as mean ± s.d. For **c**, statistical significance was attributed to values of  $P < 0.05$  as determined by unpaired  $t$ -test with Welch's correction. Individual symbols in **d–f** represent three technical replicates on RNA pooled from 6 organoids (biological replicates) per condition. Statistical analysis for **d–f,h,i** was determined at a value of  $P < 0.05$  as determined by one-way ANOVA with Tukey's multiple-comparisons test. \* $P < 0.05$ , \*\* $P < 0.01$ , \*\*\* $P < 0.001$ .



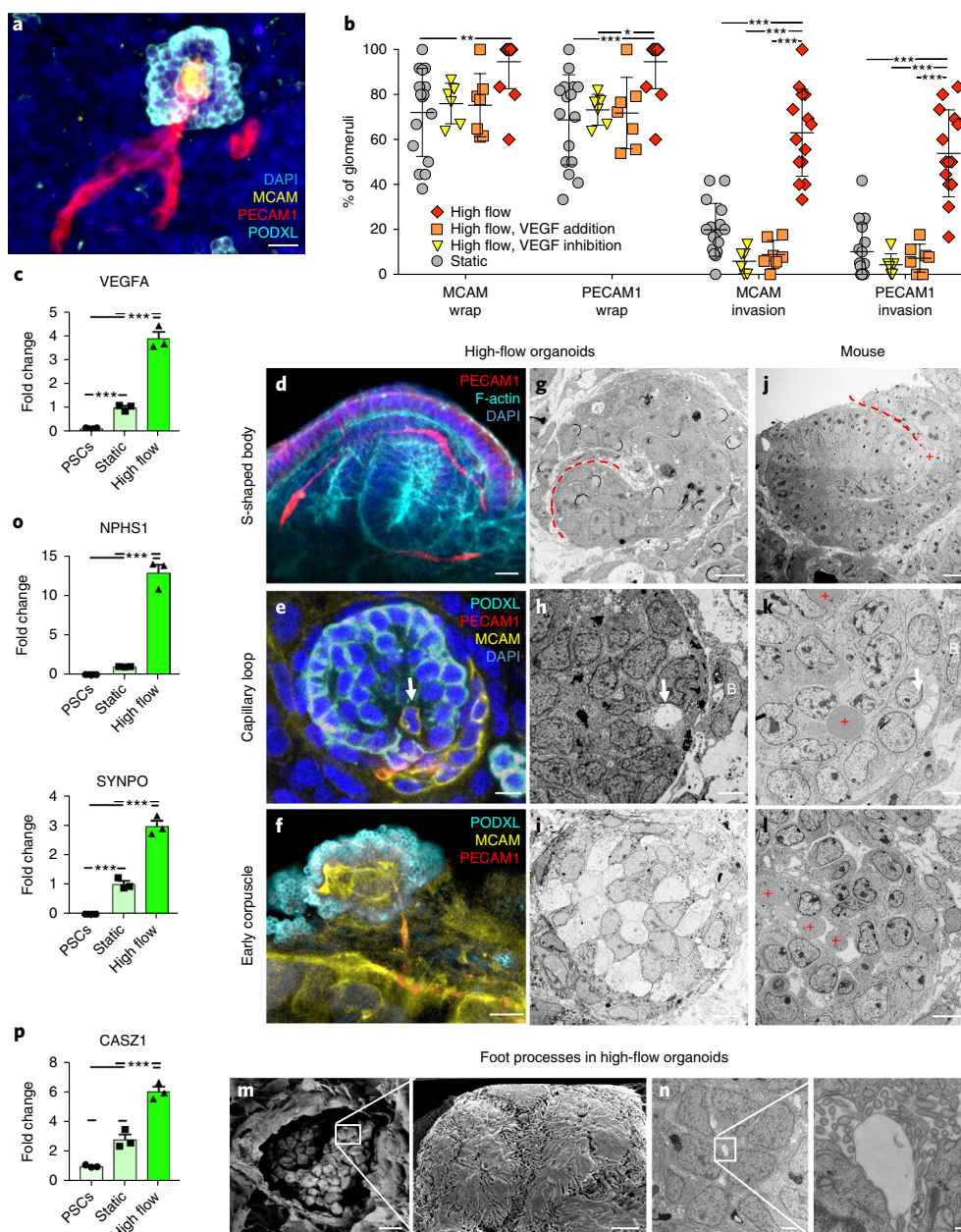


**Fig. 4 | Flow-enhanced glomerular vascularization and morphogenesis of kidney organoids in vitro mirrors stages of glomerular development in vivo.**

**a**, A 3D-rendered confocal image of vascular invasion in a PODXL<sup>+</sup> cluster showing afferent and efferent vessels. Scale bar, 40  $\mu$ m. **b**, The percentage of PODXL<sup>+</sup> clusters that exhibited vascular wrapping or invasion under static and high-FSS conditions with or without VEGF (addition or inhibition), representing whole organoids of sample size 16, 6, 7, and 14 for static, high-flow VEGF addition, high-flow VEGF inhibition, and high-flow conditions, respectively. **c**, qPCR of VEGFA at day 21. **d**, A 3D-rendered confocal image of capillary invasion in an SSB in a vascularized organoid under high FSS in vitro (day 21). Scale bar, 10  $\mu$ m. **e**, Single confocal z-slice showing capillary invasion with a PECAM1<sup>+</sup>MCAM<sup>+</sup> cell (white arrow) and MCAM<sup>+</sup> vascular precursors (CD146<sup>+</sup> cells). Scale bar, 10  $\mu$ m. **f**, MCAM<sup>+</sup>PECAM1<sup>+</sup> glomerular tuft-like formation shown as a single z-slice from a confocal image. Scale bar, 10  $\mu$ m. **g-i**, Transmission electron microscopy (TEM) images of structures correlating with the immunofluorescence images in kidney organoids (day 21). Scale bars, 4  $\mu$ m (**g,h**) or 10  $\mu$ m (**i**). **j-l**, Corresponding stages in E14.5 mouse kidneys. Red dashed lines depict clefts, white arrows denote capillary invasion, and red plus signs denote RBCs. B, Bowman's capsule-like structure. Scale bars, 8  $\mu$ m (**j,k**) or 50  $\mu$ m (**l**). **m**, TEM images of a glomerular-like structure in organoids cultured under high FSS (day 21) showing a parietal membrane enclosing a visceral cluster of cells (left), which manifest interdigitating cytoplasmic projections extending across and into the plane of field under higher magnification (right). Scale bars, 10  $\mu$ m (left) or 1  $\mu$ m (right). **n**, TEM images of a glomerulus-like compartment in organoids cultured under high FSS (day 21) (left) in which higher magnification shows podocyte foot processes abutting a glomerular tuft-like formation (right). Scale bars, 2  $\mu$ m (left) or 200 nm (right). **o,p**, qPCR for podocyte foot process proteins (**o**) and an adult transcription factor (**p**). DAPI, 4',6-diamidino-2-phenylindole; MCAM, CD146; PECAM1, CD31; PODXL, podocalyxin; SYNPO, synaptopodin; NPHS1, nephrin; PDGFR $\beta$ , platelet-derived growth factor receptor- $\beta$ ; VEGFA, vascular endothelial growth factor A; CASZ1, castor zinc finger 1. All data are plotted as mean  $\pm$  s.d. For **b**, statistical significance was attributed to values of  $P < 0.05$  as determined by two-way ANOVA with Tukey's multiple-comparisons test. Individual symbols in **c,o,p** represent three technical replicates on RNA pooled from 6 organoids (biological replicates) per condition. Statistical analysis for **c,o,p** was determined at a value of  $P < 0.05$  as determined by one-way ANOVA with Tukey's multiple-comparisons test. \* $P < 0.05$ , \*\* $P < 0.01$ , \*\*\* $P < 0.001$ .

of new blood vessels that sprout from pre-existing vessels)<sup>18,19</sup>. In the developing mammalian kidney *in vivo*, fate mapping shows that KDR<sup>+</sup> (FLK1) cells serve as EPCs that transform into intermediate MCAM<sup>+</sup> cells and, ultimately, PECAM1<sup>+</sup> mature endothelia<sup>20,21</sup> (Fig. 2a). Akin to metanephric mesenchyme *in vivo*<sup>22</sup>, KDR<sup>+</sup> EPCs were concurrently induced *in vitro* with SIX2<sup>+</sup>PAX2<sup>+</sup>SALL1<sup>+</sup> nephron progenitor cells that differentiate into the epithelial cell types of the nephron (Supplementary Figs. 6 and 7). Under high FSS, KDR<sup>+</sup> EPCs increased in number to 11.2% of the cell population in whole organoids, compared with 4.25% in static culture on chip (Fig. 2b, Supplementary Fig. 8). Moreover, transcripts for KDR and MCAM were upregulated after 10 d of high flow (differentiation day 21) (Fig. 2c,d), further indicating that FSS is an important environmental cue to expand vascular potential. Meanwhile, the expression of PDGFR $\beta$  was upregulated under high flow (Fig. 2e), where recruitment of PDGFR $\beta$ <sup>+</sup> pericyte-like cells to PECAM1<sup>+</sup> networks was consistent with vessel maturation (Fig. 2f). As the vasculature within these kidney organoids evolved *in vitro*, we noted heterogeneous expression of vascular precursor and mature markers, including areas that were MCAM<sup>+</sup>, PECAM1<sup>+</sup>, or MCAM<sup>+</sup>PECAM1<sup>+</sup> after 10 d of perfusion (differentiation day 21) (Fig. 2g, Supplementary Fig. 9). We observed open circular structures that lacked nuclei (DAPI<sup>-</sup>) and were surrounded by MCAM<sup>+</sup> and PECAM1<sup>+</sup> regions, which are indicative of lumens with varying diameter, reflecting multiscale vessel formation (Fig. 2h). Notably, we observed analogous structures in both hPSC-derived kidney organoids exposed to high FSS (Fig. 2i,j) and kidneys from mice aged embryonic day 14.5 (E14.5; Fig. 2k). To explore whether this embedded vasculature was perfusable, we carried out time-lapse live-cell monitoring of kidney organoids cultured *in vitro* under high FSS, and stained the vascular endothelium with *Ulex europaeus* I lectin. These experiments, carried out within minutes after the introduction of fluorescent beads (100-nm diameter) to the flowing media, confirmed luminal perfusion in a subset of peripheral vessels (Supplementary Fig. 10, Supplementary Video 2). To determine the extent of perfusable vasculature in whole kidney organoids, we first superfused fluorescent beads in media for several hours, then acquired live confocal images (z-stack) at the base of the organoid embedded in ECM. The organoids were then fixed, immunostained for PECAM1, and coregistered with fiducial markers. We observed the presence of beads in locations coincident with larger PECAM1<sup>+</sup> vessels, several hundred micrometers from the superfused surface (Fig. 2l,m, Supplementary Fig. 11). We also observed branched PECAM1<sup>+</sup> networks that contained terminal sprout-like structures, which lacked a PDGFR $\beta$ <sup>+</sup> cell lining, suggestive of angiogenesis (Supplementary Fig. 12a,b). We found that kidney organoids fused in as little as 24 h in culture under high FSS (Supplementary Video 3) and that robust vascular networks arose between adjacent organoids on chip (Fig. 2n). The association of PECAM1<sup>+</sup> networks with ACTA2<sup>+</sup> smooth-muscle-like cells suggests maturation of arterial lineage cells<sup>23</sup>, whereas the venous marker EMCN stains presumptive venous lineage cells (Supplementary Fig. 12c,d). Thus, kidney organoids subjected to the appropriate combination of adherent ECM, culture media, and FSS *in vitro* form increasingly mature, perfusable vasculature of varying size and lineage.

**Tubular epithelia exhibit enhanced maturation under flow.** Under static conditions, kidney organoids develop more limited vasculature, and tubular epithelia often have immature gene expression profiles with morphology analogous to that of first-trimester kidney<sup>3,9,10</sup>. After subcapsular transplantation to a mouse kidney, progressive morphogenesis of tubular structures occurs, as evident by polarization, the formation of a brush border, and ciliary assembly *in vivo*<sup>10</sup>. Native kidneys rely on extensive fluid flow both within and between tubular, interstitial, and vascular compartments to facilitate reabsorption of ~99% of the glomerular filtrate. We hypothesized that

a similar progressive morphogenesis and maturation of gene expression profiles may occur in hPSC-derived tubular cells *in vitro* when they are subjected to high FSS. Indeed, we found that the polarity of tubules formed *in vitro* was enhanced, with apical enrichment of the brush border marker *Lotus tetragonolobus* lectin (LTL) (Fig. 3a, Supplementary Fig. 13a–d) after 10 d (differentiation day 21) of culture under high FSS. Similarly, we found that primary cilia were apically enriched from 50% in static culture to 89% of LTL<sup>+</sup> cells under high FSS (Fig. 3b,c, Supplementary Fig. 13e–j). Consistent with polarization and maturation-associated ciliary assembly, the expression of ciliary proteins (PKD1, PKD2, NPHP1, NPHP6, PKHD1) was upregulated (Fig. 3d). Concurrently, expression of tubular epithelial transporters including AQP1, solute transporters (SLC34A1, ATP1A1, SLC6A19, SLC9A3, SLC2A2), and drug transporters (ABCB1, LRP2) was upregulated compared with that in static controls and undifferentiated hPSCs (Fig. 3e, Supplementary Fig. 14), indicative of enhanced functional potential. The maturation of tubular epithelial cells was evident from the upregulation of adult transcription factors (BNC2, NPAS2, TRPS1) (Fig. 3f), which are reported as mature proximal tubule markers by single-cell RNA-seq in adult human kidneys<sup>9</sup>. We quantified the association between PECAM1<sup>+</sup> networks and LTL<sup>+</sup> tubules by using confocal imaging rendered with Imaris surface functions, distance transformation, and masking tools (Fig. 3g), and found that for organoids cultured under high FSS, the percentage of vascular surface area in contact with tubules was increased by nearly threefold compared with that in organoids in static culture (Fig. 3h, Supplementary Fig. 15). Additionally, the mean distance between a given LTL<sup>+</sup> tubule and the nearest blood vessel decreased ~70% under high FSS (Fig. 3i). We observed this enhanced tubule–vascular association in both transverse and longitudinal orientations (Fig. 3j,k, Supplementary Video 4). Notably, we found that the maintenance of endogenous VEGF gradients in organoids cultured *in vitro* was crucial for vascular–tubular interactions. For example, the close association of LTL<sup>+</sup> tubules and blood vessels was disrupted when 100 ng/ml of VEGF or a VEGF inhibitor (bevacizumab<sup>24</sup> at 250  $\mu$ g/ml) was added to the media during the first 10 d of high-FSS culture, causing reversion to the tubule–vascular association observed for organoids in static culture (Fig. 3h,i, Supplementary Fig. 15). In short, organoid culture under fluid flow *in vitro* supports the maturation and morphogenesis of tubular epithelia in kidney organoids, probably as a result of interlineage endothelial–epithelial communication<sup>13</sup>.

**Glomerular vascularization and maturation *in vitro* mirror early stages of development *in vivo*.** The glomerular structures of kidney organoids in static culture are largely avascular<sup>2,3,9,25</sup>. After transplantation of a kidney organoid into an animal, host-derived vascularization promotes glomerular vascularization<sup>10</sup>. To determine whether FSS-induced vascularization of organoids *in vitro* extends to glomerular compartments, we used confocal imaging to quantify PODXL<sup>+</sup> podocyte clusters invaded by MCAM<sup>+</sup> and PECAM1<sup>+</sup> vascular structures in static and high-FSS conditions (Fig. 4a,b, Supplementary Fig. 16). Under high FSS, MCAM<sup>+</sup> and PECAM1<sup>+</sup> vascular invasion and wrapping of PODXL<sup>+</sup> clusters was significantly increased (MCAM,  $P < 0.01$ ; PECAM1,  $P < 0.001$ ; two-way ANOVA with Tukey's multiple-comparisons test; Fig. 4b). Notably, invasion was greater than 60% in high-FSS samples, compared with 10–20% in static controls (Fig. 4b), consistent with the requirement of vascular flow for glomerular assembly in animal studies<sup>26</sup>. Given that we observed significant upregulation of VEGF-A expression in organoids cultured under high FSS ( $P < 0.001$ , one-way ANOVA with Tukey's multiple-comparisons test; Fig. 4c), we postulated that these samples could be used to elucidate the role of VEGF in glomerular vascularization *in vitro*. Both VEGF inhibition (250  $\mu$ g/ml bevacizumab<sup>24</sup> for 10 d on chip) and VEGF addition (100 ng/ml for 10 d on chip) significantly reduced the incidence of invasion of



PODXL<sup>+</sup> glomeruli-like compartments by PECAM1<sup>+</sup> and MCAM<sup>+</sup> vascular networks under high FSS ( $P < 0.001$ , two-way ANOVA with Tukey's multiple-comparisons test; Fig. 4b). As the vessel percent area under high-flow conditions remained unchanged between endogenous VEGF, VEGF-addition, and VEGF-inhibition conditions, the difference in glomerular vascularization cannot be attributed to an increased abundance of vasculature (Supplementary Fig. 17, Supplementary Table 3). Unlike the random sporadic growth observed for organoids cultured in exogenously disrupted gradients, the reduced junctional density and increased average vessel length seen in unperturbed media conditions suggest that vessels grow toward an endogenous VEGF gradient (Supplementary Fig. 17b,c). The endogenous upregulation of VEGF under high FSS (Fig. 4c) appears to generate gradients that allow vessels to reach glomerulus-like compartments in time to invade rather than wrap Bowman's capsule-like structures within these kidney organoids in vitro.

Vascularization of glomeruli in vivo commences with the invasion of an S-shaped body (SSB) by a single capillary loop around which podocytes coalesce, with the formation of a primitive Bowman's capsule (capillary loop stage (CLS)), followed by vascular expansion to form nascent glomerular tufts in early corpuscles<sup>27</sup>. After 10 d of organoid culture under high FSS (differentiation day 21), glomeruli in vitro varied in a spectrum between SSBs, CLS, and early-corpuscle-like structures. Consistent with vascular invasion of an SSB, a PECAM1<sup>+</sup> vessel invaded a cleft in an SSB-like structure (Fig. 4d, Supplementary Video 5a). Meanwhile, the 'luminal' feature of an MCAM<sup>+</sup>PECAM1<sup>+</sup> vessel invading a PODXL<sup>+</sup> cellular cluster, surrounded by a putative Bowman's capsule, suggests CLS-like developing glomeruli (Fig. 4e, Supplementary Video 5). Renal-corpuscle-like structures contained MCAM<sup>+</sup>PECAM1<sup>+</sup> vasculature suggestive of capillary loops (Fig. 4f, Supplementary Fig. 16b, Supplementary Video 6). Transmission electron microscopy showed analogous structures between developing glomeruli in high-FSS organoids and E14.5 mouse kidneys, revealing that in vitro organoids may follow in vivo glomerular development through SSB, capillary loop, and early corpuscle stages (Fig. 4g–l). Capillary-loop-like structures in organoid glomeruli in vitro showed open lumens without red blood cells, which are present in capillary loops in mice (Fig. 4h–l). Scanning electron microscopy showed a thin-layered capsular structure suggestive of a parietal layer of epithelial cells (Bowman's capsule) that contained round cellular bodies with elongated cytoplasmic projections indicative of a visceral layer of epithelium (podocytes) (Fig. 4m). Similar to E14.5 embryonic mouse kidneys and human adult kidneys, grapelike clusters of visceral epithelial cells in organoids under high flow consisted of round cellular bodies with interdigitating foot-process-like structures (Supplementary Fig. 18). The cytoplasmic projections, consisting of primary stalks and secondary side branches, appeared to be polarized and abutted thin-layered membranes of capillary-loop-like structures (Fig. 4n, Supplementary Fig. 19), consistent with foot processes. Compared with those under static conditions, the foot-process-like structures seemed more prominent under high FSS, with significant upregulation of *NPHS1* (nephrin) and *SYNPO* (synaptopodin), encoding foot-process-associated proteins ( $P < 0.001$ , one-way ANOVA with Tukey's multiple-comparisons test; Fig. 4o, Supplementary Fig. 20a–d). Further, these structures fused in response to doxorubicin, as observed for foot processes in mammalian kidneys (Supplementary Fig. 20e). Concurrently, transcriptional maturation was evident from enhanced expression of podocyte adult transcription factors (WT1, CASZ1, CUX1, TEAD1)<sup>9</sup> (Fig. 4p, Supplementary Fig. 14b) with accompanying appropriate expression of the housekeeping gene *GAPDH* among all PCR samples (Supplementary Fig. 14c,d). These observations indicate that organoids cultured under high FSS show enhanced glomerular vascularization and foot process maturation, which is required to facilitate functional morphogenesis of podocytes in vitro.

## Discussion

Kidney organoids subjected to high FSS during development in vitro showed a notable enhancement in the abundance of vasculature and increased maturity in their tubular and glomerular compartments, along with concomitant morphogenesis of tubular epithelial cells and podocytes. FSS is the key parameter driving our biological findings; however, other chemomechanical cues arising from the underlying ECM, flow profile, or media composition can work collectively. Although our method does not yet ensure that the microvascular networks present in these kidney organoids will be readily perfusable, the ability to promote their flow-enhanced development in vitro opens new avenues for investigating organogenesis, nephrotoxicity, tubular and glomerular disease, and kidney regeneration with a simple microfluidic chip. Our findings could be applicable to other organoid types<sup>28–30</sup> that might similarly benefit from controlled fluid flow during development from embryonic to more functional organ equivalents in vitro.

## Online content

Any methods, additional references, Nature Research reporting summaries, source data, statements of data availability and associated accession codes are available at <https://doi.org/10.1038/s41592-019-0325-y>.

Received: 9 October 2018; Accepted: 21 December 2018;

Published online: 11 February 2019

## References

- Morizane, R. & Bonventre, J. V. Generation of nephron progenitor cells and kidney organoids from human pluripotent stem cells. *Nat. Protoc.* **12**, 195–207 (2017).
- Morizane, R. et al. Nephron organoids derived from human pluripotent stem cells model kidney development and injury. *Nat. Biotechnol.* **33**, 1193–1200 (2015).
- Takasato, M. et al. Kidney organoids from human iPS cells contain multiple lineages and model human nephrogenesis. *Nature* **526**, 564–568 (2015).
- Lam, A. Q. et al. Rapid and efficient differentiation of human pluripotent stem cells into intermediate mesoderm that forms tubules expressing kidney proximal tubular markers. *J. Am. Soc. Nephrol.* **25**, 1211–1225 (2014).
- Freedman, B. S. et al. Modelling kidney disease with CRISPR-mutant kidney organoids derived from human pluripotent epiblast spheroids. *Nat. Commun.* **6**, 8715 (2015).
- Morizane, R. & Bonventre, J. V. Kidney organoids: a translational journey. *Trends Mol. Med.* **23**, 246–263 (2017).
- Taguchi, A. et al. Redefining the in vivo origin of metanephric nephron progenitors enables generation of complex kidney structures from pluripotent stem cells. *Cell Stem Cell* **14**, 53–67 (2014).
- Takasato, M. & Little, M. H. A strategy for generating kidney organoids: recapitulating the development in human pluripotent stem cells. *Dev. Biol.* **420**, 210–220 (2016).
- Wu, H. et al. Comparative analysis of kidney organoid and adult human kidney single cell and single nucleus transcriptomes. *bioRxiv* Preprint at <https://www.biorxiv.org/content/early/2017/12/11/232561> (2017).
- van den Berg, C. W. et al. Renal subcapsular transplantation of PSC-derived kidney organoids induces neo-vasculogenesis and significant glomerular and tubular maturation in vivo. *Stem Cell Rep.* **10**, 751–765 (2018).
- Takebe, T. et al. Vascularized and complex organ buds from diverse tissues via mesenchymal cell-driven condensation. *Cell Stem Cell* **16**, 556–565 (2015).
- Bantounas, I. et al. Generation of functioning nephrons by implanting human pluripotent stem cell-derived kidney progenitors. *Stem Cell Rep.* **10**, 766–779 (2018).
- Camp, J. G. et al. Multilineage communication regulates human liver bud development from pluripotency. *Nature* **546**, 533–538 (2017).
- Kolesky, D. B. et al. 3D bioprinting of vascularized, heterogeneous cell-laden tissue constructs. *Adv. Mater.* **26**, 3124–3130 (2014).
- Homan, K. A. et al. Bioprinting of 3D convoluted renal proximal tubules on perfusable chips. *Sci. Rep.* **6**, 34845 (2016).
- Halt, K. J. et al. CD146<sup>+</sup> cells are essential for kidney vasculature development. *Kidney Int.* **90**, 311–324 (2016).
- Zudaire, E., Gambardella, L., Kurcz, C. & Vermeren, S. A computational tool for quantitative analysis of vascular networks. *PLoS One* **6**, e27385 (2011).
- Munro, D. A. D., Hohenstein, P. & Davies, J. A. Cycles of vascular plexus formation within the nephrogenic zone of the developing mouse kidney. *Sci. Rep.* **7**, 3273 (2017).

19. Daniel, E. et al. Spatiotemporal heterogeneity and patterning of developing renal blood vessels. *Angiogenesis* **21**, 617–634 (2018).
20. Robert, B., St John, P. L. & Abrahamson, D. R. Direct visualization of renal vascular morphogenesis in Flk1 heterozygous mutant mice. *Am. J. Physiol.* **275**, F164–F172 (1998).
21. McMahon, A. P. Development of the mammalian kidney. *Curr. Top. Dev. Biol.* **117**, 31–64 (2016).
22. Abrahamson, D. R. Development of kidney glomerular endothelial cells and their role in basement membrane assembly. *Organogenesis* **5**, 275–287 (2009).
23. Scheppke, L. et al. Notch promotes vascular maturation by inducing integrin-mediated smooth muscle cell adhesion to the endothelial basement membrane. *Blood* **119**, 2149–2158 (2012).
24. Wu, S., Kim, C., Baer, L. & Zhu, X. Bevacizumab increases risk for severe proteinuria in cancer patients. *J. Am. Soc. Nephrol.* **21**, 1381–1389 (2010).
25. Sharmin, S. et al. Human induced pluripotent stem cell-derived podocytes mature into vascularized glomeruli upon experimental transplantation. *J. Am. Soc. Nephrol.* **27**, 1778–1791 (2016).
26. Serluca, F. C., Drummond, I. A. & Fishman, M. C. Endothelial signaling in kidney morphogenesis: a role for hemodynamic forces. *Curr. Biol.* **12**, 492–497 (2002).
27. Ichimura, K. et al. Morphological process of podocyte development revealed by block-face scanning electron microscopy. *J. Cell. Sci.* **130**, 132–142 (2017).
28. Huch, M., Knoblich, J. A., Lutolf, M. P. & Martinez-Arias, A. The hope and the hype of organoid research. *Development* **144**, 938–941 (2017).
29. Oxburgh, L. & Carroll, T. J. The bioengineered kidney: science or science fiction? *Curr. Opin. Nephrol. Hypertens.* **25**, 343–347 (2016).
30. Little, M. H. Growing kidney tissue from stem cells: how far from “party trick” to medical application? *Cell Stem Cell* **18**, 695–698 (2016).

## Acknowledgements

The authors thank P. Galichon for flow cytometry analyses; Y. Yoda and K. Susa for cell culture and immunocytochemistry; S. Jain at The Washington University Kidney Translational Research Center (KTRC; St. Louis, MO, USA) for providing the BJFF hiPSC line; A. Moisan, C. Chen, and S. Uzel for insightful discussions; J. Weaver, B. Roman-Manso, N. Zhou, and M. Ericsson for imaging assistance; and L. Sanders for videography. This study was supported by the US National Institutes of Health (NIH; T32 fellowship training grant DK007527 to N.G.; Subaward U01DK107350 to M.T.V.; R37 grant DK039773 to J.V.B.; UG3 grant TR002155 to J.V.B., M.T.V., J.A.L., and R.M.; grant P30 DK079333 (the BJFF line) supporting The Washington University KTRC), the Harvard Stem Cell Institute (interdisciplinary grant to N.G.; seed grant to R.M. and

J.A.L.), Brigham and Women's Hospital (Research Excellence Award to N.G. and R.M.; Faculty Career Development Award to R.M.), the NIDDK Diabetic Complications Consortium (DiaComp, <https://www.diacomp.org>; grant DK076169 to R.M.), the NIH (Re)Building a Kidney Consortium (U01DK107350 to K.A.H. and J.A.L.), the Office of Naval Research Vannevar Bush Faculty Fellowship program (award no. N000141612823 to M.S.-S. and J.A.L.), and the Wyss Institute for Biologically Inspired Engineering (D.B.K., K.T.K., D.M., and J.A.L.). J.A.L. thanks the GETTYLAB and S. Lindenfeld for their generous donations in support of this research. The content is solely the responsibility of the authors and does not necessarily represent the official views of the National Institutes of Health.

## Author contributions

K.A.H., N.G., J.A.L., R.M., D.B.K., and J.V.B. conceived the project. K.A.H., N.G., and K.T.K. designed the research, and R.M. and J.A.L. supervised the research. K.A.H., N.G., K.T.K., R.M., and D.B.K. designed, performed, and analyzed all experiments. M.T.V. provided critical insights into embryonic development, cell sources, and mouse embryonic kidneys. M.S.-S. designed and built the silicone millifluidic chips, interfacing with perfusion pumps, and analyzed the fluid flow profiles on chip. D.M. and T.M. sourced and validated antibodies, optimized staining protocols, and provided invaluable cell culture analysis and support. T.F. developed methodology for quantifying vascular and tubule features in confocal imaging stacks. All authors contributed to manuscript writing.

## Competing interests

J.V.B. and R.M. are co-inventors on patents (PCT/US16/52350) on organoid technologies that are assigned to Partners Healthcare. J.V.B. or his family has received income for consulting from companies interested in biomarkers: Sekisui, Millennium, Johnson & Johnson, and Novartis. J.V.B. is a co-founder of, is a consultant to, and owns equity in Goldfinch Bio. K.A.H. is a co-founder and chairwoman of NanoHybrids Inc. J.A.L. is a co-founder of and owns equity in Voxel8 Inc.

## Additional information

**Supplementary information** is available for this paper at <https://doi.org/10.1038/s41592-019-0325-y>.

**Reprints and permissions information** is available at [www.nature.com/reprints](http://www.nature.com/reprints).

**Correspondence and requests for materials** should be addressed to J.A.L. or R.M.

**Publisher's note:** Springer Nature remains neutral with regard to jurisdictional claims in published maps and institutional affiliations.

© The Author(s), under exclusive licence to Springer Nature America, Inc. 2019



## Methods

**Millifluidic chip fabrication.** We used a silicone-based ink to 3D-print customized perfusion gaskets (Supplementary Fig. 1), in which developing kidney organoids were placed on an engineered ECM layer (1 mm thick) and subjected to a controlled-FSS environment. The ink was composed of a two-part silicone elastomer (SE 1700, Dow Chemical) with a 10:1 base-to-catalyst ratio (by weight) and was homogenized with a centrifugal mixer for 2 min (2,000 r.p.m.; AE-310, Thinky Corp, Japan). The silicone ink was printed within 2 h of being mixed with catalyst. This ink was loaded in a syringe (EFD Inc., East Providence, RI, USA) and centrifuged to remove any air bubbles before printing at room temperature. The chips were fabricated using a custom-designed, multimaterial 3D bioprinter equipped with four independently addressable printheads mounted on a three-axis, motion-controlled gantry with a build volume of 725 × 650 × 125 mm (AGB 10000, Aerotech Inc., Pittsburgh, PA, USA). The silicone (PDMS) ink was housed in a syringe barrel to which a 410- $\mu$ m-diameter nozzle was attached via a luer lock (EFD Inc., East Providence, RI, USA). Ink was extruded through deposition nozzles by applied air pressure (800 Ultra dispensing system, EFD Inc., East Providence, RI, USA) ranging from 10 to 90 p.s.i., corresponding to print speeds between 1 mm/s and 5 cm/s. The customized perfusion chip gasket was printed by deposition of the silicone ink through a tapered 410- $\mu$ m nozzle onto 50 × 75 mm glass slides. The gasket tool path was created with a custom MATLAB script that generates G-code for a final gasket structure. After printing, the perfusion chip was cured at 80 °C in an oven for >1 h, stored at room temperature, and autoclaved before use. The organoid chamber was 15 mm wide by 3.6 mm high and 60 mm long; the ECM was placed on the base of the perfusion gasket and was 1 mm thick. The organoids (between 4 and 20 per chip) were placed centrally in an area 8 mm wide by 3.6 mm high and 20 mm long as shown in Supplementary Fig. 1d.

**Engineered extracellular matrix preparation and rheology.** The ECM comprised a gelatin network. To prepare the ECM components, the user first produces a 15% (w/v) gelatin solution (Type A, 300 bloom from porcine skin; Sigma) by adding gelatin powder to a warm solution (70 °C) of DPBS (1× Dulbecco's PBS without  $\text{Ca}^{2+}$  and  $\text{Mg}^{2+}$ ). The gelatin is stirred for 12 h at 70 °C, and the pH is then adjusted to 7.5 with 1 M NaOH. The solution is sterile-filtered and stored at 4 °C in aliquots for later usage (<3 months). A fibrinogen solution (50 mg/ml) is made from lyophilized bovine blood plasma protein (Millipore) dissolved at 37 °C in sterile DPBS without  $\text{Ca}^{2+}$  and  $\text{Mg}^{2+}$ . The solution is held at 37 °C without agitation for at least 45 min to allow complete dissolution. The transglutaminase solution (60 mg/ml) is made from lyophilized powder (Moo Gloo, TI) dissolved in DPBS without  $\text{Ca}^{2+}$  and  $\text{Mg}^{2+}$  and gently mixed for 20 s. The solution is then held at 37 °C for 20 min and sterile-filtered before use. A  $\text{CaCl}_2$  stock solution (250 mM) is prepared from  $\text{CaCl}_2$  pellets dissolved in sterile water. For the preparation of stock solutions of thrombin, lyophilized thrombin (Sigma Aldrich) is reconstituted at 500 U/ml in sterile water and stored at -20 °C. Thrombin aliquots are thawed immediately before use.

Before a layer of engineered ECM is cast in the 3D-printed chip, several components are mixed in advance at appropriate concentrations, including 10 mg/ml fibrinogen, 2 wt% gelatin, 2.5 mM  $\text{CaCl}_2$ , and 0.2 wt% transglutaminase. This solution is then equilibrated at 37 °C for 15–20 min before use to improve the optical clarity of the ECM<sup>15</sup>. Next, the solution is rapidly mixed with stock thrombin solution at a ratio of 250:1, resulting in a final thrombin concentration of 2 U/ml. Within 2 min at 37 °C, soluble fibrinogen cures to a fibrin gel. For this reason, the ECM solution must be cast onto the base of the perfusion chip immediately after being mixed with thrombin. The gasket with ECM is then placed in a sterile container and kept in the incubator for a minimum of 30 min before assembly with housing, media, and pretubular aggregate integration.

A controlled stress rheometer (DHR-3, TA Instruments, New Castle, DE, USA) with a 40-mm-diameter, 2° cone and plate geometry was used to measure the rheological properties of the ECM. The shear storage ( $G'$ ) and loss ( $G''$ ) moduli were measured at a frequency of 1 Hz and an oscillatory strain ( $\gamma$ ) of 0.01. For time sweeps, a premixed ECM solution containing thrombin was rapidly placed onto the Peltier plate held at 37 °C. The  $G'$  of the final cured engineered ECM was approximately 800 Pa.

To prepare the ECM formulations shown in Supplementary Fig. 2, we used fibrin at either 10 mg/ml or 25 mg/ml with thrombin at 2 U/ml and 2.5 mM  $\text{CaCl}_2$ . The fibrin–Col I ECM was prepared from fibrinogen solution mixed at a final concentration of 25 mg/ml with collagen I (rat tail collagen I, Corning; 1 mg/ml) at pH 7.5, a thrombin concentration of 2 U/ml, and 2.5 mM  $\text{CaCl}_2$ . Matrigel (Corning) was diluted by 50% with sterile PBS and cured at 37 °C.

We also made and evaluated another ECM formulation that included fibrin along with human umbilical vein endothelial cells (HUVECs) and human neonatal dermal fibroblast cells (HNFs) (Supplementary Fig. 3b). We prepared the preformed network of HUVECs and HNFs by combining HUVECs and HNFs at a 5:1 ratio at a concentration of 2 million cells/ml in 10 mg/ml fibrin gel. The cells were cultured in 1:1 DMEM:endothelial growth medium 2 (EGM2; Lonza) plus 5% FBS for 3 d to allow spontaneous tubulogenesis to occur before pretubular aggregates were loaded on top of the fibrin gel supporting the HUVEC:HNF network. At this point, the media was changed to 1:1 EGM2:ARPMI (Advanced Roswell Park Memorial Institute medium + 1× GlutaMAX) and held in static conditions for 7 d.

**Organoid assembly and perfusion on printed millifluidic chips.** For assembly of the kidney organoids-on-chip, pretubular aggregates (with ages between 11 and 14 d) in media were pipetted onto the top of the ECM on gasket in the window region highlighted in Supplementary Fig. 1d. A large number of organoids can fit on chip, and we typically used between 4 and 20 per run, but upward of 100 or more can fit if needed. The organoids were randomly spaced within the window of 8 × 20 mm; note that the distance between the organoid surface on the ECM and the upper acrylic lid was 2.6 mm. The gasket was then placed into a machined stainless steel base. Stainless steel tubes (Microgroup, Inc.; grade 304, gauge 18RW; ends were de-burred before use) were pushed through the PDMS at the inlet and outlet and positioned such that they were above the ECM surface. Finally, a thick acrylic lid was placed on top (Supplementary Fig. 1a–e). The lid and base were clamped together by four screws, forming a seal around the printed silicone gasket. Next, sterile two-stop peristaltic tubing (PharMed BPT) was filled with media and connected to the outlet of a sterile filter that was attached to a 10-ml syringe barrel (EFD Nordson), which served as a media reservoir. Organoid media (ARPMI + 1× GlutaMAX + 1.5% FBS and 1% antimycotic/antibiotic solution) that had equilibrated for >3 h in an incubator at 37 °C, 5%  $\text{CO}_2$  was added to the media reservoir, and tubing from the reservoir was connected to the inlet of the chip (metal hollow perfusion pin). Tubing was also connected to the outlet of the chip through its respective stainless steel pin. A syringe was then used to exert slight pressure on the media in the barrel, forcing it to enter and completely fill the open gasket area, with extra care taken to not disturb the pretubular aggregates. Hose pinch-off clamps were added at the inlet and outlet of the perfusion chip to prevent uncontrolled flow when disconnected from the peristaltic pump. To complete the closed perfusion circuit, we connected tubing from the outlet to the media reservoir. The media reservoir was equilibrated with atmospheric conditions in the incubator at all times by means of a sterile filter on top of the media reservoir. Media was changed every 2–3 d. The typical volume of media per organoid on chip and static on ECM was 0.5–0.8 ml. The typical volume of media per organoid in U-wells was 0.2 ml. We determined that a volume of media per organoid in the range of 0.2–1 ml per organoid had no measurable effect on the resulting vasculature on chip in high-flow conditions (Supplementary Fig. 5). Furthermore, we measured organoid height in order to understand the dynamic changes evolving on chip during organoid development. We found that kidney organoids under low and high FSS initially flattened, then grew to heights greater than those of U-well controls. Thus, gross morphologic height changes are not a dominant variable controlling the enhancement in vascularization, as the heights were similar in low- and high-FSS conditions by day 21, whereas the vasculature was dramatically enhanced in high-FSS samples only (Fig. 1 and Supplementary Fig. 22).

We used an Ismatec IPC-N low-speed peristaltic pump to direct media into the gasket in a closed-loop circuit at volumetric flow rates ranging from 40  $\mu$ l/min to 4.27 ml/min. During the first 12–24 h of culture on chip, pretubular aggregates were subjected to low flow rates of 40  $\mu$ l/min or less. These extremely low flow rates provided nutrient supply without high shear stresses that could have broken the connection forming between the aggregates and the ECM below. After 24 h, the aggregates were strongly adherent to the ECM, and the volumetric flow rate ( $Q$ ) was increased to between 1.0 and 4.27 ml/min.

**Flow profile analysis.** Flow modeling was done with COMSOL Multiphysics simulation software. We calculated the fluid flow velocity profile by assuming a Stoke's flow, using a 1 ml/min volumetric flow rate. The channel comprised the curved surface of the gel, the silicone walls at the two sides, and the perfusion chip lid. For direct measurement of FSS at the gel–channel interface, fluorescent beads were tracked within the organoid seeding region at various volumetric flow rates. To visualize the flow, we mounted millifluidic chips onto a confocal microscope stage and perfused them with PBS containing 0.4% (v/v) of a 2% solids solution of 0.5- $\mu$ m 488-nm fluorescent beads (Thermo Fisher). The pump was connected to the chip via 18.2 m of loosely spooled silicone tubing (Cole-Parmer peroxide-cured silicone tubing; 1/32-inch inner diameter × 3/32-inch outer diameter) to dampen pulsatility to obtain a time-averaged shear stress. Analysis was performed along an 8-mm-long transverse line centered on the midline of the channel and the organoid seeding region at two-thirds of the distance between the inlet and the outlet of the perfusion chip. Confocal videos of bead flow were captured using a window of 600  $\mu$ m along the channel by 90  $\mu$ m across. To estimate the velocity gradient for calculating shear stress at the gel–channel interface, we captured four videos at 40- $\mu$ m height intervals just above the gel surface. We extracted the mean bead velocity at each height by performing a cross-correlation of the video frames in a direction parallel to the bead flow. The peak location of the cross-correlation represents the mean displacement of the beads over the time frame of the two images used for cross-correlation. The cross-correlation time frame was increased until the peak in the cross-correlation of the video was less than 6 s.d. of the noise floor. The velocity was calculated as the ratio of the cross-correlation peak displacement and the time difference between the two frames used for cross-correlation. Velocities were calculated for each frame of the video, and averaged. The velocity gradient was measured using linear regression of the mean velocities at the four different heights. The FSS was then calculated as the product of the gradient and a dynamic viscosity of 0.78 cP for DMEM at 37 °C (ref. <sup>31</sup>). To measure the flow pulsatility, we removed the 18.2 m of silicon tubing

and replaced it with the standard 10 cm of tubing between the pump and chip. A 50-s video was captured at the midline of the channel, two-thirds of the distance between the inlet and the outlet, and the bead velocity was measured over time via the cross-correlation method described above (Supplementary Fig. 1e–g). The predicted flow profile obtained with COMSOL and direct measurements from bead flow were in good agreement if we assumed a rectangular cross-section. Wall FSS in flow through a rectangular cross-section ( $\tau$ ) is calculated with the equation  $\tau = 6\mu Q/bh^2$ , where  $\mu$  is the medium viscosity,  $b$  is the channel width, and  $h$  is the channel height (the empty channel through which fluid flows is approximated as a rectangular cross-section ( $b = 14$  mm;  $h = 2.6$  mm) where the organoids reside). In this study, we varied the volumetric flow rates to induce a low FSS that ranged from  $1 \times 10^{-7}$  to  $1 \times 10^{-4}$  dyn/cm<sup>2</sup> and a high FSS that ranged from  $8 \times 10^{-3}$  to  $3.5 \times 10^{-2}$  dyn/cm<sup>2</sup>. Note that one can reduce the channel dimensions simply by increasing the ECM height, which yields a higher FSS at a given volumetric flow rate. We have constructed channel heights as small as  $b = 0.5$  mm, leading to FSS at  $\sim 1$  dyn/cm<sup>2</sup>, and organoids cultured on this chip showed enhancements in vascularity and in tubular and glomerular maturation comparable to those of organoids subjected to an FSS ranging from  $8 \times 10^{-3}$  to  $3.5 \times 10^{-2}$  dyn/cm<sup>2</sup>.

**Cell culture.** H9 human embryonic stem cells (ESCs; WiCell) and BJFF human induced PSCs (provided by Prof. Sanjay Jain at Washington University) were maintained in feeder-free culture with StemFit Basic02 (Ajinomoto Co., Inc.) supplemented with 10 ng/ml FGF2 (Peprotech) as previously reported<sup>1</sup>. Human glomerular microvascular endothelial cells (GMECs) expressing RFP (Angio-Proteomie) were cultured with EGM2 media (Lonza) and used up to passage 9. HUVECs expressing RFP (Angio-Proteomie) were cultured with EGM2 media (Lonza) and used up to passage 9. HNDs expressing GFP (Angio-Proteomie) were cultured per the supplier's instructions and used up to passage 15.

**Organoid preparation and culture.** Organoid preparation is covered in detail elsewhere<sup>1</sup>, but briefly, hPSCs were differentiated into metanephric mesenchyme cells that included SIX2<sup>+</sup> nephron progenitor cells with approximately 80–90% efficiency by a three-step directed differentiation protocol<sup>1</sup> (Fig. 1a, bottom). Metanephric mesenchyme cells were differentiated into pretubular aggregates in suspension culture, and then the aggregates were transferred onto the chip (Fig. 1a, top) anytime between days 11 and 14 of differentiation (Supplementary Fig. 2g). Further differentiation into kidney organoids was stimulated by the same directed differentiation protocol, reported previously, except that 1.5% FBS (heat inactivated; Gibco) was added<sup>1</sup>. This same process can be used to massively scale up kidney organoid production in Elplasia culture plates, which have patterned microwells (Kuraray) (Supplementary Fig. 21). With traditional methods, kidney organoids will contain roughly 100,000 cells per aggregate. However, within the same footprint as a single well in a six-well plate, approximately 1,000 mini-organoids can be produced, containing approximately 5,000 cells per aggregate. Notably, when these mini-organoids were placed within our engineered microenvironment on chip, they behaved similarly to larger organoids and developed enhanced vascularization under high-FSS conditions.

We explored several experimental conditions that did not lead to enhanced vascularization. In particular, the addition of adult human primary GMECs, either by aggregation with nephron progenitor cells at day 8 or placement of the cells in culture on ECM near renal aggregates or vesicles, was not successful (Supplementary Fig. 3a). Either the developing kidney organoids failed to form properly at day 8 or HUVECs, HNDs, and adult GMECs failed to integrate within the forming organoid, respectively (Supplementary Fig. 3b).

**Doxorubicin exposure.** The chemotherapeutic drug doxorubicin (Sigma) was dosed at 10  $\mu$ M for 24 h from day 20 to day 21 of culture in either static or high-FSS conditions.

**Bead perfusion.** At day 21 of differentiation in either static or perfused conditions, we added 100-nm fluorescent beads to the media (FluoSpheres from Thermo Fisher; carboxylate terminated) at a dilution of 1:1,000. For the static case, the organoids were gently shaken in the incubator for 3 h in the presence of bead-laden media. For the perfused conditions, the kidney organoids-on-chip were perfused with bead-laden media under high-FSS conditions for 3 h in the incubator. Because of the high degree of light scattering by the tissue, we used a two-step method employing fiduciary markers to facilitate bead visualization within the whole organoids. We then imaged the kidney organoids by confocal microscopy to determine the distribution of the fluorescent beads within them. Fiduciary markers in the sample were used to ensure that after fixing, washing, and staining for PECAM1 (CD31), the same confocal z-stack was collected with endothelial markers and could be properly correlated with bead location. Note that the beads were nearly completely flushed out during the washing and primary and secondary staining processes. Z-stack images and reconstructions were rendered (Fig. 2l,m, Supplementary Fig. 11). Although we found that the beads nonspecifically bound to both static and perfused organoids, they concentrated in larger luminal CD31<sup>+</sup> structures and were observed in those luminal spaces throughout the entire depth of those organoids under high-FSS conditions.

To obtain a live perfusion bead movie, we used slightly different techniques. First, live imaging requires a very bright and lasting stain of the vasculature. We

tried live tagging of CD31 and CD146 with fluorophore-conjugated antibodies, but the signal was not strong. We switched to a rhodamine-conjugated agglutinin (ULEX: *Ulex europaeus* agglutinin I (UEA I) from Vector Laboratories) because its signal overlaps with both CD31 and CD146. As scattering from thick organoid tissue and nonspecific deposition of superfluorescent beads were known problems, we imaged the vessels live within the first 15 min of bead perfusion. We imaged near the bottom of the organoid, close to the glass; perfusion is likely to be limited in this region compared with that at the top of the organoid, but so is nonspecific bead uptake. Before imaging we perfused in ULEX at a 1:200 dilution in media. ULEX was quickly rinsed away with fresh media at a 3 $\times$  volume dilution and replaced with media and beads at a 1:1,000 dilution. Imaging was carried out for 900 frames with 400 ms between frames, and halfway through the ULEX laser was turned off in order to capture the bead flow alone on chip. The video was rendered at 20 frames per second (Supplementary Video 2, Supplementary Fig. 10).

**Flow cytometry.** The preparation of live cells for flow cytometry required several digestion steps. First, the organoids (10–15 per condition) were cut away from the ECM and placed in a 15-ml Falcon tube. Excess media was removed, and the sample was washed with PBS without Ca<sup>2+</sup> and Mg<sup>2+</sup>. Next, 100  $\mu$ l of 2.5% trypsin (Corning) in 10 mM EDTA (Sigma-Aldrich) was added for 2 min at 37 °C. Then 1.9 ml of PBS without Ca<sup>2+</sup> and Mg<sup>2+</sup> was added and the tube was centrifuged at 300g for 4 min. The supernatant was aspirated, 200  $\mu$ l of collagenase IV (STEMCELL Technologies) was added, and the suspension was pipetted to further break up the organoid. The samples were incubated for 10 min at 37 °C. After more pipetting, 5 ml of PBS was added and samples were centrifuged at 300g for 4 min. The supernatants were aspirated and the cells were incubated on ice for 30 min with FLK1-555 (Bioss) at a 1:10 dilution in PBS without Ca<sup>2+</sup> and Mg<sup>2+</sup>. The samples were washed three times with PBS without Ca<sup>2+</sup> and Mg<sup>2+</sup> and then suspended in either DAPI (Sigma) or SYTOX Red (Thermo Fisher; 1:1,000 dilution) in BD FACS flow buffer in a total of 300  $\mu$ l of fluid. Samples were sent through a Falcon 70- $\mu$ m filter before being analyzed by flow cytometry (BD LSRFortessa), and data were collected from  $n = 100,000$  cells per sample. All gates used to ensure that live, homogeneous cells were counted are shown in Supplementary Figs. 7 and 8. Note that in Supplementary Fig. 8d,f we observed a bimodal population of large and small cell sizes for day 21 kidney organoids. KDR<sup>+</sup> EPCs were found predominantly in the small-cell fraction.

**qRT-PCR.** Kidney organoids were manually extracted from perfusable chips by pipette. RNA was isolated from kidney organoid samples with TRIzol (Invitrogen) according to the manufacturer's protocol. A minimum of six organoids were used per sample. cDNA was synthesized with a high-capacity cDNA reverse-transcription kit (Applied Biosystems). Quantitative real-time PCR was carried out with iTaq SYBR Green supermix (Bio-Rad) and a Bio-Rad iQ5 multicolor real-time PCR detection system. Primer sequences were designed using FASTA sequences (PubMed) and verified with Primer3, and one of the primers from the pairs of primers was designed to include an exon–exon junction. Target genes were normalized to glyceraldehyde 3-phosphate dehydrogenase (*GAPDH*) expression. The mRNA expression was calculated via the  $2^{-\Delta\Delta Ct}$  method, expressed as an  $n$ -fold difference relative to expression in the control group, and reported with s.e. Of note, cDNA quality was confirmed by DNA gel electrophoresis of the housekeeping gene *GAPDH* across samples (Supplementary Fig. 14c). A full primer list can be found in Supplementary Table 1.

**Obtaining mouse embryonic kidneys.** All procedures were in accordance with the NIH Guide for the Care and Use of Laboratory Animals and were approved by Institutional Animal Care and Use Committees at Brigham and Women's Hospital. Embryonic kidneys at stage E14.5 (day of plug = E0.5) were isolated from timed pregnant females (Charles River).

**Electron microscopy.** For transmission electron microscopy, kidney organoids or mouse embryonic kidneys were fixed in place with 2.5% glutaraldehyde, 1.25% paraformaldehyde, and 0.03% picric acid in 0.1 M sodium cacodylate buffer, pH 7.4, for a minimum of several hours. Small samples (1  $\times$  1 mm) were excised and washed in 0.1 M cacodylate buffer and bathed in 1% osmium tetroxide (OsO<sub>4</sub>) (EMS) and 1.5% potassium ferrocyanide (K<sub>3</sub>Fe(CN)<sub>6</sub>) (Sigma) for 1 h, washed in water three times and incubated in 1% aqueous uranyl acetate (EMS) for 1 h followed by two washes in water and subsequent dehydration in varying grades of alcohol (10 min each; 50%, 70%, 90%, 2  $\times$  10 min 100%). The organoids or mouse kidneys were then put in propyleneoxide (EMS) for 1 h and incubated overnight in a 1:1 mixture of propyleneoxide and TAAB Epon (Marivac Canada Inc.). The following day the samples were embedded in TAAB Epon and polymerized at 60 °C for 48 h. Ultrathin sections (about 60 nm) were cut on a Reichert Ultracut-S microtome, placed on copper grids, stained with lead citrate, and examined in a JEOL 1200EX transmission electron microscope, and images were recorded with an AMT 2k CCD (charge-coupled device) camera.

For scanning electron microscopy, kidney organoids or mouse kidneys were again fixed in place with 2.5% glutaraldehyde, 1.25% paraformaldehyde, and 0.03% picric acid in 0.1 M sodium cacodylate buffer, pH 7.4, for a minimum of several hours. They were then washed three times with PBS until picric acid (yellow

color) was washed out. Organoids and mouse kidneys were placed in a solution of 30% sucrose in PBS for 1 h. Then that solution was removed and replaced with a 1:1 mixture of 30% sucrose solution in PBS:optimal cutting temperature (OCT) freezing medium (Electron Microscopy Science) for 30–45 min at room temperature. Organoids were then set in a cryomold for freezing, excess fluid was removed, and OCT was placed on top to fill in the mold. The organoids were frozen and placed in the  $-20^{\circ}\text{C}$  freezer overnight. The samples were then cut in a cryotome in 5- $\mu\text{m}$  sections (Thermo Fisher), mounted on glass slides, and stained with hematoxylin and eosin. Once the opening to Bowman's capsules was visible, sectioning was ceased. We then unembedded the organoids from the OCT by heating the samples to  $40^{\circ}\text{C}$  and physically removing them from OCT, washed them extensively with water, and dehydrated the tissue. Subsequent dehydration in varying grades of ethanol was required (20 min each; 30%, 50%, 70%, 90%,  $3 \times 20$  min 100%). The samples were then placed in 50% ethanol and 50% hexamethyldisilazane (HMDS) for 30 min followed by 100% HMDS for three rounds of 30 min each. All steps were performed in a closed glass container. After the final washing with HMDS, the samples were removed and placed in an open container in the fume hood to dry. Dried samples were mounted to aluminum pin mounts with conductive carbon tape, sputter-coated with 5 nm of gold or platinum, and imaged with an UltraPlus field emission scanning electron microscope (Zeiss) at 1 keV.

**Immunostaining.** We used immunostaining followed by confocal microscopy to assess the localization of cellular or extracellular proteins within or adjacent to organoids. Prior to immunostaining, each organoid sample was washed with PBS and then fixed for 1 h with 10% buffered formalin. The fixative was removed by several washes in PBS for several hours, and samples were then blocked overnight with 1 wt% donkey serum in PBS with 0.125 wt% Triton X-100. Primary antibodies to the protein or biomarker of interest were incubated with the constructs for 2 d at  $4^{\circ}\text{C}$  at the dilutions listed in Supplementary Table 2 in a solution of 0.5 wt% BSA and 0.125 wt% Triton X-100. Removal of unbound primary antibodies was accomplished via a wash step against a solution of PBS or 0.5 wt% BSA and 0.125 wt% Triton X-100 in PBS for 1 d. Secondary antibodies were incubated with the constructs for several hours at 1:500 dilution in a solution of 0.5 wt% BSA and 0.125 wt% Triton X-100 in PBS. Samples were counterstained with DAPI and then washed for at least several hours in PBS before imaging. A full antibody list can be found in Supplementary Table 2.

**Image rendering and analysis.** Phase contrast microscopy was carried out on an inverted Leica DM IL scope with objectives ranging from  $1.25\times$  to  $40\times$ . Confocal microscopy was done on an upright Zeiss LSM 710 with water-immersion objectives ranging from  $10\times$  to  $40\times$  and spectral lasers at wavelengths of 405, 488, 514, 561, and 633 nm. Image reconstructions of z-stacks were generated in Imaris using the z-projection function with the maximum pixel intensity setting. Any increases in brightness were applied uniformly across an entire z-projected image. 3D image reconstructions and rotating movies also were generated with Imaris software. The CytoSMART (Lonza) incubator system was used to capture time-lapse imaging (Supplementary Video 2). Confocal z-stacks were used to count the percentage of ciliated cells (Fig. 3c),  $>64$  counts per condition including 4 biological replicates, and the amount of PODXL<sup>+</sup> clusters that were invaded or wrapped by vascular cells (Fig. 4b, Supplementary Fig. 16),  $n > 14$  biological replicates per condition, over 4 independent experiments for high-flow and static conditions and  $n$  between 6 and 16 biological replicates (whole organoids) per condition over 2 independent experiments for VEGF inhibition and addition.

**AngioTool analysis.** Confocal z-stacks of PECAM1 were taken of fixed whole-mount organoids, both iPSC- and ESC-derived, in the various culture conditions.

The z-stacks were taken at the limit of the confocal depth with each sample, nearly 250  $\mu\text{m}$  per sample, which represents approximately the same volume per organoid analyzed. Those z-stacks were then flattened in ImageJ to a 2D maximum-intensity projection (as required by the AngioTool for input). The default settings were used on the AngioTool for analysis, and vessel diameters of 4, 7, 10, and 14 were analyzed for each organoid. In all cases, the whole organoid was used for analysis.

**Imaris analysis.** Confocal z-stacks of PECAM1 and LTL were taken of fixed whole-mount organoids, both iPSC- and ESC-derived, in the various culture conditions. The z-stacks were taken at the limit of the confocal depth with each sample, roughly 250  $\mu\text{m}$  per sample, which represents approximately the same volume per organoid analyzed. Those z-stacks were then opened in Imaris imaging software. As shown in Supplementary Fig. 15, the confocal 3D rendering was turned into a vascular surface and a tubule surface. Then we used the Imaris surface contact area XTension to quantify the percent overlap between the vascular and tubular surfaces in 3D; values are reported in Fig. 3h. For assessment of the average distance from the vasculature to a tubule, first the Imaris distance transformation XTension was run on the tubule surface. The resulting channel was then masked by the vascular surface to create a new masked distance transformation channel. That masked distance transformation channel was sent to Fiji (ImageJ) to retrieve a histogram of the masked voxels, from which we obtained a geometric mean for each sample, reported in Fig. 3i.

**Statistics and reproducibility.** Data in all bar charts and dot plots are expressed as mean  $\pm$  s.d. Statistical analysis was done in MATLAB and GraphPad Prism 7, and statistical significance was attributed to values of  $P < 0.05$  as determined by ANOVA analysis, as described in the figure legends. Different significance levels ( $P$  values) are indicated in each figure with asterisks: \* $P < 0.05$ , \*\* $P < 0.01$ , \*\*\* $P < 0.001$ .  $P$  values for Supplementary Fig. 17c are summarized in Supplementary Table 3. For transparency, we state here the number of times experiments were repeated independently, with similar results obtained, to produce the data shown: Fig. 1b, 6; Fig. 1c–l, 15; Fig. 1m, 4; Figs. 1n, 1; Fig. 2b, 2; Fig. 2c–e, 1; Fig. 2f–h, 15; Fig. 2i–k, 5; Fig. 2l,m, 9; Fig. 2n, 10; Fig. 3a,b, 3; Fig. 3c, 3; Fig. 3d–f, 1; Fig. 3g, 15; Fig. 3h,i, 2; Fig. 3j,k, 5; Fig. 4a, 15; Fig. 4b, 3; Fig. 4c, 1; Fig. 4d–l, 15; Fig. 4m, 15; Fig. 4n, 15; Fig. 4o,p, 1; Supplementary Fig. 1f,g, 2; Supplementary Fig. 2a–f, 6; Supplementary Fig. 2h,i, 15; Supplementary Fig. 3a,b, 2; Supplementary Fig. 4a–l, 4; Supplementary Figs. 5–8, 2; Supplementary Fig. 9, 15; Supplementary Figs. 10 and 11, 9; Supplementary Fig. 12a,b, 15; Supplementary Fig. 12c,d, 2; Supplementary Fig. 13a–j, 3; Supplementary Fig. 14a–d, 1; Supplementary Fig. 16a,b, 15; Supplementary Fig. 17a, 3; Supplementary Fig. 17b,c, 4; Supplementary Fig. 18a–d,f, 15; Supplementary Fig. 19, 15; Supplementary Fig. 20, 3; Supplementary Fig. 21, 10; Supplementary Fig. 22, 3; Supplementary Video 2, 9; Supplementary Videos 3–6, 15.

**Reporting Summary.** Further information on research design is available in the Nature Research Reporting Summary linked to this article.

## Data availability

The data generated in this study are available from the corresponding authors upon request.

## References

- Ainslie, K. M., Garanich, J. S., Dull, R. O. & Tarbell, J. M. Vascular smooth muscle cell glycocalyx influences shear stress-mediated contractile response. *J. Appl. Physiol.* **98**, 242–249 (2005).



## Reporting Summary

Nature Research wishes to improve the reproducibility of the work that we publish. This form provides structure for consistency and transparency in reporting. For further information on Nature Research policies, see [Authors & Referees](#) and the [Editorial Policy Checklist](#).

### Statistical parameters

When statistical analyses are reported, confirm that the following items are present in the relevant location (e.g. figure legend, table legend, main text, or Methods section).

n/a Confirmed

- ☐ ☒ The exact sample size ( $n$ ) for each experimental group/condition, given as a discrete number and unit of measurement
- ☐ ☒ An indication of whether measurements were taken from distinct samples or whether the same sample was measured repeatedly
- ☐ ☒ The statistical test(s) used AND whether they are one- or two-sided  
*Only common tests should be described solely by name; describe more complex techniques in the Methods section.*
- ☒ ☐ A description of all covariates tested
- ☒ ☐ A description of any assumptions or corrections, such as tests of normality and adjustment for multiple comparisons
- ☐ ☒ A full description of the statistics including central tendency (e.g. means) or other basic estimates (e.g. regression coefficient) AND variation (e.g. standard deviation) or associated estimates of uncertainty (e.g. confidence intervals)
- ☐ ☒ For null hypothesis testing, the test statistic (e.g.  $F$ ,  $t$ ,  $r$ ) with confidence intervals, effect sizes, degrees of freedom and  $P$  value noted  
*Give  $P$  values as exact values whenever suitable.*
- ☒ ☐ For Bayesian analysis, information on the choice of priors and Markov chain Monte Carlo settings
- ☒ ☐ For hierarchical and complex designs, identification of the appropriate level for tests and full reporting of outcomes
- ☒ ☐ Estimates of effect sizes (e.g. Cohen's  $d$ , Pearson's  $r$ ), indicating how they were calculated
- ☐ ☒ Clearly defined error bars  
*State explicitly what error bars represent (e.g. SD, SE, CI)*

Our web collection on [statistics for biologists](#) may be useful.

### Software and code

Policy information about [availability of computer code](#)

Data collection

No specific codes were used to collect data. Data was collected using standard brightfield and confocal imaging, qPCR, and flow cytometry machines.

Data analysis

Data analysis of the data collected (see above) was performed using standard commands in Excel 2016 and plotting/statistics were performed in Graphpad Prism 7 software. qPCR primers were designed using Primer3 (version 4.1.0). For millifluidic chip fabrication, the gasket tool-path was created using a custom MATLAB script. Flow modeling was performed using COMSOL Multiphysics simulation software. G code was used to program an Aerotech 3D stage to print the silicon gaskets. The Fiji (ImageJ) plugin Angiotool was used to analyze abundance and character of vasculature. Imaris software was used to analyze in 3D the vascular and tubule surfaces and quantify their relative overlap and distance from each other using confocal z stack images as an input.

For manuscripts utilizing custom algorithms or software that are central to the research but not yet described in published literature, software must be made available to editors/reviewers upon request. We strongly encourage code deposition in a community repository (e.g. GitHub). See the Nature Research [guidelines for submitting code & software](#) for further information.

## Data

Policy information about [availability of data](#)

All manuscripts must include a [data availability statement](#). This statement should provide the following information, where applicable:

- Accession codes, unique identifiers, or web links for publicly available datasets
- A list of figures that have associated raw data
- A description of any restrictions on data availability

Regarding the availability of data, no publicly available datasets were used, supplementary figures 7 and 8 include raw flow cytometry data with gating strategy, and there are no restrictions to data availability - please directly contact the corresponding author.

## Field-specific reporting

Please select the best fit for your research. If you are not sure, read the appropriate sections before making your selection.

☒ Life sciences ☐ Behavioural & social sciences ☐ Ecological, evolutionary & environmental sciences

For a reference copy of the document with all sections, see [nature.com/authors/policies/ReportingSummary-flat.pdf](https://www.nature.com/authors/policies/ReportingSummary-flat.pdf)

## Life sciences study design

All studies must disclose on these points even when the disclosure is negative.

Sample size	Sample size was determined by number of independent kidney organoids used per sample. No statistical method was used to pre-determine sample size, rather mirrored animal experiments with each independent organoid treated as a littermate. The sample size was sufficient for our claims based on statistical significance.
Data exclusions	No data was excluded from the analyses.
Replication	Measures taken to verify the reproducibility of the experimental findings include analyses based on individual organoids, all organoids across samples generated from the same batch of nephron progenitor cells and immunostained simultaneously for each experiment, and then repeating experiments across organoids generated from multiple batches of nephron progenitor cells were performed. All attempts at replication were successful.
Randomization	Samples (organoids) were allocated to the different experimental groups completely randomly with each new batch of nephron progenitor cells.
Blinding	Investigators were not blinded to group allocation during data collection and analysis. As identical gains and exposure times were used in fluorescent imaging during data collection when quantitative comparisons were made, and identical thresholds were applied during unbiased data analysis using FIJI/ImageJ/Imaris, blinding was not required for the data generated from immunostaining. The gating strategies for flow cytometry are depicted in the raw data provided in supplemental figures.

## Reporting for specific materials, systems and methods

### Materials & experimental systems

n/a	Involved in the study
<input type="checkbox"/>	<input checked="" type="checkbox"/> Unique biological materials
<input type="checkbox"/>	<input checked="" type="checkbox"/> Antibodies
<input type="checkbox"/>	<input checked="" type="checkbox"/> Eukaryotic cell lines
<input checked="" type="checkbox"/>	<input type="checkbox"/> Palaeontology
<input type="checkbox"/>	<input checked="" type="checkbox"/> Animals and other organisms
<input checked="" type="checkbox"/>	<input type="checkbox"/> Human research participants

### Methods

n/a	Involved in the study
<input checked="" type="checkbox"/>	<input type="checkbox"/> ChIP-seq
<input type="checkbox"/>	<input checked="" type="checkbox"/> Flow cytometry
<input checked="" type="checkbox"/>	<input type="checkbox"/> MRI-based neuroimaging

## Unique biological materials

Policy information about [availability of materials](#)

Obtaining unique materials	The unique material used in this study relates to human pluripotent stem cell-derived kidney organoids. The kidney organoids were generated from the H9 human embryonic stem cell line available from WiCell and the directed differentiation protocol from human stem cells to kidney organoids has been published in Nature Biotech (Morizane et al, 2015) and Nature Protocols
----------------------------	---

(Morizane et al, 2017). We also used the iPSC line BJFF provided by Sanjay Jain as discussed in the methods section of the manuscript. All unique materials are readily available from the authors.

## Antibodies

Antibodies used	<p>Antibody, Source Catalog #, Host Species, Reactivity Concentration</p> <p>MCAM, Abcam, ab75769, Rabbit, anti-human, 1:250</p> <p>PODXL, R&amp;D Systems, AF1658, Goat, anti-human, 1:250</p> <p>PECAM1, Abcam, ab9498, Mouse, anti-human, 1:250</p> <p>EMCN, Sigma-Aldrich, SAB4502163, Rabbit, anti-human, 1:250</p> <p>PDGFR<math>\beta</math>, Abcam, ab32570, Rabbit, anti-human, 1:250</p> <p>Col IV, Abcam, ab52235, Rabbit, anti-human, 1:250</p> <p>ATP1A1, Abcam, ab76020, Rabbit, anti-human, 1:250</p> <p>TUBA4A, Abcam, ab24610, Mouse, anti-human, 1:250</p> <p>SIX2, Proteintech, 11562, Rabbit, anti-human, 1:500</p> <p>SALL1, R&amp;D Systems, PP-K9814-00, Mouse, anti-human, 1:100</p> <p>PAX2, Covance, PRB-276P, Rabbit, anti-human, 1:500</p> <p>aSMA, Abcam, Ab5964, Rat, anti-human, 1:250</p> <p>FLK1-555, Bioss, bs-10412R, anti-Human, 1:10</p>
Validation	<p>All antibodies used were validated for the application used (IHC, ICC, flow cytometry) according to manufacturers' websites. Validation statements for the species and application on the manufacturer's website are listed below. Antibodies were further chosen based on having references in the literature, and include many antibodies used and reported in our labs prior work published in Nature affiliated journals.</p> <p>ab75769: Reacts with: Mouse, Rat, Human, Suitable for ICC/IF, IHC-Fr, WB, IHC-P, Flow Cyt.</p> <p>AF1658: Reacts with Human, Suitable for WB, Flow Cyt., IHC</p> <p>ab9498: Reacts with Mouse, Human, Cynomolgus monkey, Suitable for IHC-Fr, ICC/IF, Flow Cyt, WB, IHC-P.</p> <p>SAB4502163: Reacts with rat, mouse, human, Suitable for ELISA, IF.</p> <p>ab32570: Reacts with Mouse, Rat, Human, Suitable for IHC-Fr, Flow Cyt, IHC-FoFr, WB, IHC-P, ICC/IF, IP, IHC-FrFI.</p> <p>ab52235: Reacts with mouse, human, Suitable for IHC, WB, ELISA.</p> <p>ab76020: Reacts with mouse, rat, human, tilapia, Suitable for ICC/IF, WB, Flow Cyt, IHC-P.</p> <p>ab24610: Reacts with Mouse, Rat, Sheep, Human, Monkey, Sea urchin, Suitable for Flow Cyt, WB, IHC-P, ICC/IF, IHC-Fr.</p> <p>11562: Reacts with human, mouse, rat, American alligator, Suitable for WB, IP, IHC.</p> <p>PP-K9814-00: Reacts with human, Suitable for WB, ELISA. IHC application was reported in previous publications such as PMID: 24332837.</p> <p>PRB-276P: Reacts with human, mouse, chicken, xenopus, zebrafish, Suitable for WB, IHC.</p> <p>Ab5964: Reacts with human, Suitable for IHC, WB.</p> <p>bs-10412R: Reacts with human, mouse, rat, pig, Suitable for WB, FCM, IHC.</p>

## Eukaryotic cell lines

Policy information about [cell lines](#)

Cell line source(s)	H9 human embryonic stem cells are available from WiCell. BJFF iPSC line is available from Sanjay Jain upon request and MTA. GMECs, HUVECs, and HNDfs are available from Angio-Proteomie.
Authentication	The H9 cell line is authenticated by WiCell, who distributes it commercially. Washington University in Saint Louis authenticated the BJFF line. GMECs, HUVECs, and HNDfs are authenticated by Angio-Proteomie.
Mycoplasma contamination	Our H9 cell line has repeatedly tested negative for mycoplasma contamination. We run tests monthly. GMECs, HUVECs, and HNDfs are checked by Angio-Proteomie.
Commonly misidentified lines (See <a href="#">ICLAC</a> register)	No commonly misidentified cell line was used.

## Animals and other organisms

Policy information about [studies involving animals](#); [ARRIVE guidelines](#) recommended for reporting animal research

Laboratory animals	All procedures were in accordance with the NIH Guide for the Care and Use of Laboratory Animals and were approved by Institutional Animal Care and Use Committees at Brigham and Women's Hospital. Embryonic kidneys at stage E14.5 (day of plug=E0.5) were isolated from timed pregnant females (Charles River).
Wild animals	The study did not involve wild animals.
Field-collected samples	The study did not involve samples collected from the field.



## Flow Cytometry

### Plots

Confirm that:

- ☒ The axis labels state the marker and fluorochrome used (e.g. CD4-FITC).
- ☒ The axis scales are clearly visible. Include numbers along axes only for bottom left plot of group (a 'group' is an analysis of identical markers).
- ☒ All plots are contour plots with outliers or pseudocolor plots.
- ☒ A numerical value for number of cells or percentage (with statistics) is provided.

### Methodology

Sample preparation

Samples were prepared from experimentally treated kidney organoids as outlined in materials and methods. Briefly, single cell dissociation of kidney organoids was performed using a combination of enzymatic (collagenase type IV, Stemcell Technologies x30 min total incubation) and interval manual dissociation using serially reduced sizes of pipette tips.

Instrument

A BD LSR Fortessa was used in the Baeur Core at Harvard University.

Software

FloJo was used to collect and analyze the flow cytometry data.

Cell population abundance

Cells were not sorted such that no post-sort fractions existed.

Gating strategy

Rather than a description, we have included the gating strategy used for all relevant experiments in the supplementary figures, which include the preliminary FSC/SSC gates of the starting cell populations and later indicate boundaries between "positive" and "negative" staining cell populations with percentages labeled.

- ☒ Tick this box to confirm that a figure exemplifying the gating strategy is provided in the Supplementary Information.